Journal of Inflammation Research

Dovepress
Taylor & Francis Group

Open Access Full Text Article

ORIGINAL RESEARCH

Qingwen Hufei Granules Attenuate Lipopolysaccharide-Induced Acute Lung Injury by Suppressing NLRP3 Inflammasome-Dependent Pyroptosis

Kaihua Long[1,*], Yun Yang[2,*], Yuan Wang[1], Bo Wang[2], Huiying Zhou[1], Yuxi Liu[1], Ye Li[1], Shuanzhu Yang[1], Liping Cao[1], Tingting Huang[2], Yang Liu[1,3,4], Hong Zhang[1]

[1]Shaanxi Academy of Traditional Chinese Medicine (Shaanxi Provincial Hospital of Traditional Chinese Medicine), Xi'an, People's Republic of China; [2]College of Life Sciences, Northwest University, Xi'an, People's Republic of China; [3]Institute of Basic Research in Clinical Medicine, China Academy of Chinese Medical Sciences, Beijing, People's Republic of China; [4]Shaanxi Panlong Pharmaceutical Group Limited by Share Ltd., Xi'an, People's Republic of China

*These authors contributed equally to this work

Correspondence: Yang Liu; Hong Zhang, Shaanxi Academy of Traditional Chinese Medicine (Shaanxi Provincial Hospital of Traditional Chinese Medicine), No. 4 Xihuamen, Lianhu District, Xi'an, 710003, People's Republic of China, Email liuyang311111@163.com; zhanghong919919@163.com

Background: Currently, clinical treatments for ALI include vasodilators, glucocorticoids, and mechanical ventilation; however, these therapies are associated with various adverse reactions. Therefore, there is a need to develop safer and more effective treatment options. Traditional Chinese Medicine (TCM), particularly Qingwen Hufei Granules (QHG), has demonstrated efficacy in treating respiratory disorders, including upper respiratory tract infections and influenza. However, the active components and mechanism of action of QHG remain unclear.

Methods: Lipopolysaccharide (LPS) induced ALI mouse model. We analyzed the main pharmacodynamic components of QHG by HPLC, determined the effects of QHG on the cell viability and inflammatory factors of RAW264.7 cells, and recorded the body weight and lung tissue wet/dry (W/D) of ALI mice. Inflammatory factors in bronchoalveolar lavage fluid (BALF), serum, and lung tissue were determined using ELISA, and the protective effect of hematoxylin and eosin (H&E) staining of lung tissue was studied. Transcriptomic, qRT-PCR, Western blotting, immunohistochemistry, and immunofluorescence analyses were used to analyze QHG and explore the mechanism of ALI damage reduction.

Results: The findings demonstrated that QHG effectively mitigated inflammatory cell invasion and pulmonary edema. Moreover, it diminished the concentrations of IL-6, TNF-α, and IL-1β in lung tissue, serum, and BALF. Furthermore, QHG notably decreased the levels of NO, reactive oxygen species(ROS), IL-6, IL-1β, and TNF-α in the supernatants of RAW264.7 cells. Transcriptomic analysis of the lung tissue revealed that QHG primarily enriched the NOD-like receptor (NLR) signaling pathway. qRT-PCR, Western blotting, immunohistochemistry, and immunofluorescence experiments confirmed that QHG mitigated ALI damage through the NLR signaling pathway. Furthermore, seven key components in QHG were determined by using HPLC.

Conclusion: Our study demonstrated that QHG effectively mitigated LPS-induced ALI, and provided preliminary insights into its mechanism of action and material basis.

Keywords: acute lung injury, lipopolysaccharide, Qingwen Hufei granules, transcriptomics, NOD-like receptor-signaling pathway

Introduction

Acute lung injury (ALI) is a major health burden worldwide and is associated with high morbidity and mortality rates. The presenting features are acute respiratory insufficiency, rapid onset of polypnea, cyanosis resistant to oxygen therapy, and diffuse alveolar infiltrates observed on chest radiography.[1,2] Various etiologies, including acute pneumonia, sepsis,

Received: 14 March 2025
Accepted: 12 July 2025
Published: 4 August 2025

Graphical Abstract

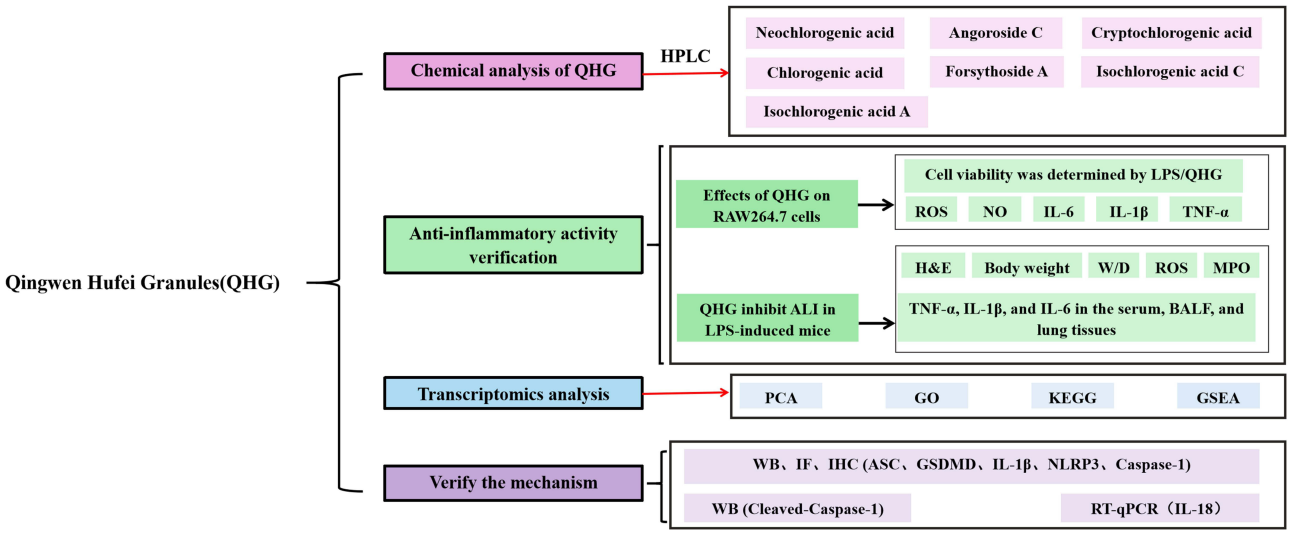

and severe trauma can cause ALI. Lipopolysaccharide (LPS), the main constituent of the cell wall of Gram-negative bacteria, is an infectious agent that causes ALI. As one of the common critical clinical conditions, ALI progresses rapidly and usually degenerates into acute respiratory distress syndrome (ARDS), characterized by acute respiratory distress and refractory hypoxemia, which can cause respiratory failure. The mortality rate of acute lung injury ranges from 33% to 55%, posing a serious threat to human health and putting immense pressure on the global burden of health resources.[3,4] Current clinical treatments for ALI include mechanical ventilation, bronchodilators, corticosteroids, antibiotics, and other supportive therapies. Unfortunately, these methods have several limitations including poor patient tolerance and multiple side effects.[5]

The "holistic concept" and "syndrome differentiation" approaches in TCM provide a particular advantage in the treatment of ALI. TCM can inhibit oxidative stress, reduce inflammation, and improve lung tissue damage, thus playing an important role in treatment of ALI.[6,7] QHG manufactured by Professor Cao Liping, a well-known TCM professional, is derived from the Chinese prescriptions "Yinqiao San", "Xuanmai Ganjie Decoction", and "Sijunzi Decoction". It contains 16 herbs, including *Lonicera japonica* Thunb. (Jinyinhua), *Forsythia suspensa* (Thunb.) Vahl (Lianqiao); *Isatis indigotica* Fort. (Daqingye), *Scrophularia ningpoensis* Hemsl. (Xuanshen), *Prunus armeniaca* L.var.ansu Maxim. (Kuxingren), *Fritillaria thunbergii* Miq. (Zhebeimu), *Platycodon grandiflorum* (Jacq.)A. DC. (Jiegeng), *Perilla frutescens* (L.) Britt. (Zisuye), *Saposhnikovia divaricata* (Turcz.) Schischk. (Fangfeng), *Atractylodes macrocephala* Koidz. (Chaobaizhu), *Poria cocos* (Schw.) Wolf (Fuling), *Artemisia capillaris* Thunb.(Yinchen), *Codonopsis pilosula* (Franch.) Nannf. (Dangshen) and *Lophatherum gracile* Brongn. (Danzhuye), *Ophiopogon japonicus* (L. f) Ker-Gawl. (Maidong) and *Glycyrrhiza uralensis* Fisch. (Gancao). We analyzed the effective chemicals in QHG collected by UHPLC-Q Exactive FocusMS/MS using our crew: terpenoids, phenylpropanoids, chromogen flavonoids, and organic acids. These components have been shown to exert anti-ALI effects.[8–10]

The primary pathological features of ALI include diffuse alveolar injury and breakdown of the endothelial barrier of microcirculation vessels. ALI is a complex inflammatory cascade that involves cell death.[11] The NLRP3 inflammasome plays a crucial role in innate immunity and maintaining microenvironmental homeostasis. However, excessive activation can lead to excessive inflammatory responses and worsening of disease progression in various inflammatory diseases.[12] During ALI, abnormally activated NLRP3 inflammasome activates Caspase-1 and Cleaves gasdermin D to form a peptide in the nitrogen-terminal active domain, which causes cell membrane rupture, releases mature IL-1β, and induces pyroptosis in macrophages.[13,14]

In this study, we established a fingerprint and content determination method for QHG by HPLC. We then analyzed the effect of QHG on inflammatory changes in RAW264.7 macrophages under LPS stimulation. Additionally, we conducted an experimental study on the pharmacodynamic and anti-inflammatory effects of QHG in an LPS-induced mouse model. Finally, we performed a transcriptomic analysis of mouse lung tissue and verified the mechanism by which QHG alleviates ALI using qRT-PCR, Western blotting, immunohistochemistry, and immunofluorescence.

In conclusion, QHG have shown remarkable efficacy in the clinical treatment of respiratory diseases. They contain multiple active ingredients that are effective against acute lung injury. However, the specific mechanism of action remains unknown, and it is worth exploring whether they exert their effects through NLRP3 inflammasome.

Our study is of great significance for the research on the treatment of acute lung injury with traditional Chinese medicine.

Materials and Methods

Reagents

LPS (*Escherichia coli* 0111:B4) was procured from Sigma-Aldrich, and Dexamethasone (LB22207, XianJu) was used in this study. The concentrations of IL-6, IL-1β, and TNF-α were quantified using enzyme-linked immunosorbent assay (ELISA) kits (Bioswamp). ROS and Myeloperoxidase(MPO) assay kits were obtained from Nanjing Jiancheng Bioengineering Institute. Antibodies NLRP3 (ab270449), GSDMD (ab219800) were purchased from Abcam. ASC (#67824) was obtained from Cell Signaling Technology, and Caspase-1 (22915-1-AP), IL-1β (26048-1-AP) were obtained from Proteintech. All antibodies were diluted at a ratio of 1:1000. β-Actin was purchased from zenbio (Chengdu, China), dilution ratio is 1:10,000.

Preparation of QHG

Qingwen Hufei granules were self-produced preparations by the Shaanxi Provincial Hospital of Chinese Medicine (Xi'an, China),10g x 6 bags/box, and identification of product 20220506.

Chemical Analysis of QHG

The QHG was finely ground, and 2.0 g was accurately weighed and placed in a 100 mL conical flask with a plug. It was dissolved in 30 mL of methanol, weighed, and treated with ultrasound (50 kHz frequency, 300 W power) for 30 min. After cooling to room temperature, the solution was shaken, filtered, and dried. The total volume was adjusted to 10 mL in a volumetric flask. Subsequently, the solution was filtered through a 0.45 μm microporous filter membrane, and the resulting filtrate was used for subsequent analyses.

Control standards were accurately weighed and placed in 10 mL volumetric flask. The volume was fixed after diluting with 50% methanol. The following compounds were used as standards: neochlorogenic acid (CHB220328), chlorogenic acid (CHB231010), cryptochlorogenic acid (CHB230830), forsythia glycoside A (CHB231017), 3,5-O-dicaffeoylquinic acid (CBH231227), 4,5-caffeoyl quinic acid (CHB240104), and angloside C (CHB240217), with a purity of ≥98%. All control products were purchased from Chengdu Cloma Biotechnology Co. Ltd.

To establish an HPLC chromatographic analysis method were conducted on an Agilent ZORBAX Eclipse Plus-C18 column (250 mm × 4.6 mm, 5 μm). The mobile phase consisted of methanol (A) and 0.1% phosphoric acid (B), with a flow rate of 0.8 mL/min, and an injection volume of 10 μL. The gradient elution sequences are listed in Table 1.

Table 1 Gradient Elution Program

Time (min)	0	12	35	38	80	95	100
A%	10	16	18	30	34	58	90

Animals and Treatments

Male C57 mice were acquired from Jiangsu Huachuang Cigna Pharmaceutical Technology Co. Ltd. (certificate no. SCXK 2020-0009). The experimental protocols for animal studies were approved by the Ethics Committee of the Shaanxi Academy of TCM (Animal Approval Number: (2022) Animal Ethical Review Number (15)). All procedures were performed in strict accordance with the Guidelines for Animal Experimentation (ARRIVE).[15] The animal experiment protocol of this study strictly adheres to the 《Guidelines for the Ethical Review of Animal Welfare》 (GB/T 35892-2018). Prior to experimentation, the mice were acclimatized for three days under controlled conditions with 12-hour light and dark cycles. SPF-grade male C57 mice, with an average weight of 22 ± 2 g, were randomly assigned to six groups (n=60): control, LPS (5 mg/kg), LPS + dexamethasone (DXM, 2 mg/kg), LPS + low-QHG (QL, 3.075 g/kg), LPS + medium-QHG (QM, 6.15 g/kg), and LPS + high-QHG (QH, 12.3 g/kg). QHG and DXM were administered via gavage for 7 days, whereas the control and LPS groups received saline. On the final day, 1.5 hours post-gavage, all groups, barring the control, were administered an intratracheal instillation of LPS.[16,17] Subsequently, the mice were euthanized using an overdose of pentobarbital sodium, and BALF, serum, and lung tissues were preserved at −80°C for analysis.

Wet/Dry Weight Ratio

The chest of each mouse was opened and the lung was removed. After separating the trachea and esophagus, the lung lobe was weighed immediately to obtain a wet mass. After euthanasia, the lungs were desiccated at 60°C for 72 h until consistent weight was achieved, and the wet-to-dry (W/D) weight ratio was calculated.[18]

Histopathologic Evaluation of Lung Tissue

The lung tissues were preserved in 4% paraformaldehyde, subjected to gradient ethanol dehydration, and embedded in paraffin. After cooling, the tissues were sectioned and stained with hematoxylin and eosin (H&E) for microscopic evaluation of pulmonary changes.[19]

Myeloperoxide (MPO) Activity and Reactive Oxygen Species (ROS) Assay

MPO activity in the lung tissues was quantified using spectrophotometric colorimetry. Tissue homogenates were prepared, cooled, and centrifuged at 4°C and 6000 rpm for 15 minutes. This was followed by additional centrifugation at 4°C and 12,000 rpm for 15 minutes. The MPO activity (U/g) was determined using the following formula:

MPO activity (U/g) = (measured OD value − control OD value) / 11.3 × sample weight.

ROS levels in the lung tissue were determined using the double-antibody sandwich method. The lung tissues were homogenized using a chilled tissue homogenizer at 3000 rpm for 20 min, after which the supernatants were separated. ROS levels were quantitatively assessed by analyzing the color intensity, which was directly correlated with the ROS concentration in the samples. OD was measured at 450 nm using a spectrophotometer.[20]

Bronchoalveolar Lavage Fluid (BALF) Analysis

After blood extraction, the mice were placed on an operating table, their chest was opened, and their lungs were ligated. Pre-cooled PBS buffer (1 mL) was injected into the trachea, and the lungs were lavaged back and forth twice to collect alveolar lavage fluid. The samples were then centrifuged at 3000 rpm for 15 min at 4°C. The resultant supernatant was examined using ELISA kits, following the manufacturer's protocols, to assess the levels of IL-6, IL-1β, and TNF-α.[21]

Levels of TNF-α, IL-6, and IL-1β in Serum

After a 72-hour period of modeling, mice were euthanized, and their eyeballs were excised. The collected supernatants were centrifuged under the same conditions, and the cytokines IL-6, IL-1β, and TNF-α were measured using ELISA kits, according to the manufacturer's instructions.[22]

Cytokine Assay

RAW264.7 cells, sourced from the Cell Resource Center at the Institute of Basic Medicine of the Chinese Academy of Medical Sciences (fifth passage), were cultured at a density of 2×10^5 cells/mL. The cell viability assay was conducted using the Cell Counting Kit-8 (CCK-8) method. The experiment included three groups: blank control (without LPS or drug), model (LPS at a final concentration of 100 ng/mL), and LPS + drug treatment (LPS at 100 ng/mL + QHG freeze-dried powder at concentrations of 5, 10, 20, 40, 80, and 160 μg/mL) groups. Each group had three to four replicates and the experiment was repeated three times. For each experimental group, the corresponding drug solution was added for 6 h, followed by addition of LPS to a final concentration of 100 ng/mL. The control group was administered an equal volume of DMEM. After 24 h of incubation, NO release in the supernatant was measured using a NO kit, and ROS production was assessed using a ROS kit. Intracellular ROS levels were quantified using flow cytometry (BECKMAN COULTER, Cytoflex). ELISA kits were used to measure the secretion of TNF-α, IL-6, and IL-1β from the supernatant.[23]

Transcriptome Analysis of Lung Tissue

Total RNA was extracted from lung tissue using the TRIzol method (Life Technologies), and RNA quality was assessed by agarose gel electrophoresis. Transcriptome libraries were constructed using mRNA purification and fragmentation, followed by cDNA first-strand synthesis, second-strand synthesis, adapter ligation, and purification of ligation products. The DNA 1000 Assay Kit (Agilent Technologies) was used for quality assessment. Differential gene expression analysis was performed using the DESeq2 package in R software.[24]

qRT-PCR Analysis

The lung tissue was lysed using Trizol, total RNA from the lung was extracted for concentration assessment, the sample was diluted, and subsequently reverse-transcribed into cDNA (condition: 20μL reaction system). qRT-PCR conditions: pre-denaturation at 95°C for 30 seconds, denaturation at 95°C for 10 seconds, annealing and elongation at 60°C for 30 seconds, with a total of 40 cycles conducted. The mRNA expression levels of IL-18 were quantified using the $2^{-\Delta\Delta Ct}$ method. The primers were synthesized by Beijing Qingke Biotechnology Co., Ltd. The sequences are shown in Table 2.

Western Blotting

Lung tissues were lysed in RIPA buffer and protein concentrations were quantified using the BCA assay. Proteins were separated by SDS-PAGE and transferred onto (lyvinylidene difluoride a PVDF) membranes. The membrane was blocked for two hours at ambient temperature and subsequently incubated with primary antibody at 4°C overnight. All the antibodies were diluted using the antibody diluent, with a dilution ratio of 1:1000. After four TBST washes, the membrane was incubated with secondary antibody for two additional hours. The protein bands were visualized using an ECL luminescent reagent, and band intensities were analyzed using the Image J software.[25]

Immunohistochemistry

Paraffin-embedded sections were sequentially deparaffinized in three different solutions for 15 min each followed by 5 min of anhydrous ethanol. Antigen retrieval was performed using a microwave in the retrieval solution for 20 minutes. After cooling, the sections were washed three times with PBS for 5 min each and treated to block endogenous peroxidase activity. Blocking was performed using bovine serum albumin (BSA) for 20 min at room temperature. The sections were incubated with primary antibodies overnight at 4°C in a humidified chamber. For DAB staining, fresh DAB solution was prepared and applied to the tissue for color development at room temperature. Color development was monitored under a microscope. The sections were counterstained with hematoxylin for 3 min, washed with tap water, and stained with blue water.[26]

Table 2 Primers Sequencing Used for mRNA Quantitation

Gene ID	Forward Primer Sequence	Reverse Primer Sequence
IL-18	5′-CCTTTGAGGCATCCAGGACA-3′	5′-GGGAACAGCCAGTGTTCAGT-3′

Immunofluorescence

Sections were prepared as described previously for immunohistochemistry. For antigen retrieval, the sections were dipped in the retrieval solution and microwaved for 20 min, followed by endogenous peroxidase blocking. After the primary antibody application, the sections were sealed with BSA for 30 min at room temperature before the application of the secondary antibody. DAPI was used for nuclear staining and the sections were incubated for 10 min. After three PBS washes, the slides were examined and imaged using fluorescence microscopy.[27]

Statistical Analysis

Data are presented as the mean ± standard deviation (SD). Statistical analysis was conducted using one-way analysis of variance (ANOVA), with statistical significance set at P-value of < 0.05. Principal component analysis (PCA) was performed using an Illumina NovaSeq X Plus system (Gene Denovo Biotechnology Co., Ltd., Guangzhou, China). Graphical representations were produced using GraphPad Prism version 9.0.

Results

Determination of Active Components in QHG

Chromatographic analysis revealed peaks 1–7, which were identified as Neochlorogenic acid, Chlorogenic acid, Cryptochlorogenic acid, Forsythoside A, Isochlorogenic acid A, Isochlorogenic acid C, and Angoroside C, respectively, and aligned with the reference substances (Figure 1A and B).

Effects of QHG on RAW264.7 Cells

LPS successfully stimulated RAW264.7 macrophages to generate an inflammatory cell model. The effect of QHG on the secretion of ROS, NO, IL-1β, TNF-α, and IL-6 in cellular supernatants was evaluated. As illustrated in Figure 2, the LPS-treated group exhibited a significant increase in ROS, NO, TNF-α, IL-6, and IL-1β levels in the supernatant. Conversely, the QHG-treated groups (20, 40, 80, and 160 μg) showed a significant reduction in ROS, IL-6, and IL-1β levels in a concentration-dependent manner.

Preventive Effects of QHG on ALI in Mice

The control group showed no abnormalities in lung tissue structure, with clear alveoli and chambers, and no hemorrhagic edema or inflammatory cell infiltration. In contrast, the model group exhibited disorganized lung tissue, an altered alveolar structure, pulmonary capillary congestion, cellular bleeding, inflammatory cell infiltration, and significant tissue damage. Compared with the model group, the lung tissue of QM-treated and QH-treated mice showed significant improvements, with near-normal alveolar structure and effective alleviation of inflammatory cell infiltration in the lung interstitium (Figure 3A). On the first day after the model was established, the body weight of the LPS group mice decreased significantly compared to the blank group. The body weight of the treatment group was significantly higher than that of the control group. On the third day, the body weight of the LPS group failed to recover and was significantly lower than that of the control group (Figure 3B). The LPS group showed a significantly increased W/D ratio (Figure 3C), ROS activity (Figure 3D), and MPO activity (Figure 3E), which was reduced in the QM, QH, and DXM treatment groups. These results suggest that LPS induces edema and cellular damage, whereas QM and QH exert significant protective effects.

QHG Attenuated Inflammation in ALI

LPS-induced ALI is characterized by elevated levels of TNF-α, IL-1β, and IL-6. These cytokines were quantified in the bronchoalveolar lavage fluid (BALF), serum, and lung tissue. ALI can cause an inflammatory response in the lungs, and this local inflammatory response can trigger the migration of inflammatory cells, which in turn leads to a systemic inflammatory response. This experiment measured the levels of inflammatory factors in the serum, lung tissue and BALF of mice. As shown in Figure 4A–C, there was a significant increase in these cytokines in the LPS group, whereas their levels were substantially decreased in the QM, QH, and DXM groups. These results indicate that QHG significantly

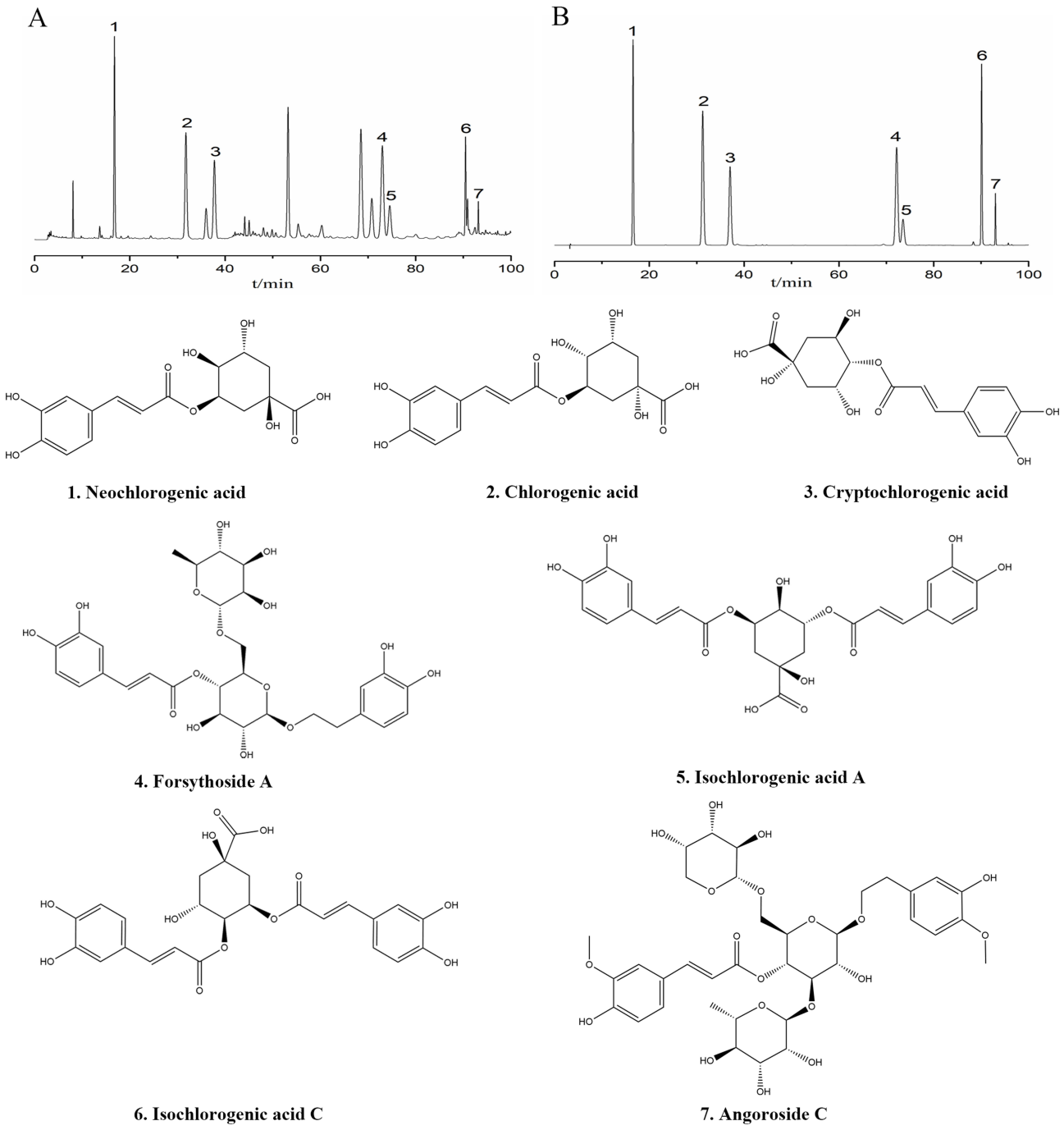

Figure 1 Chromatogram of QHG and compound structure. (**A**) QHG sample; (**B**) Mixed control sample.

alleviates ALI; therefore, we measured the levels of inflammatory cytokines in the BALF, serum, and lung tissue of mice. The results revealed that the expression of TNF-α, IL-1β, and IL-6 in the serum, BALF, and lung tissues of mice in the LPS group was significantly increased. The levels of TNF-α, IL-1β, and IL-6 in BALF, serum, and lung tissues were significantly decreased in QM, QH, and DXM (Figure 4A–C), suggesting that QHG can significantly inhibit ALI through anti-inflammatory effects.

https://doi.org/10.2147/JIR.S523490

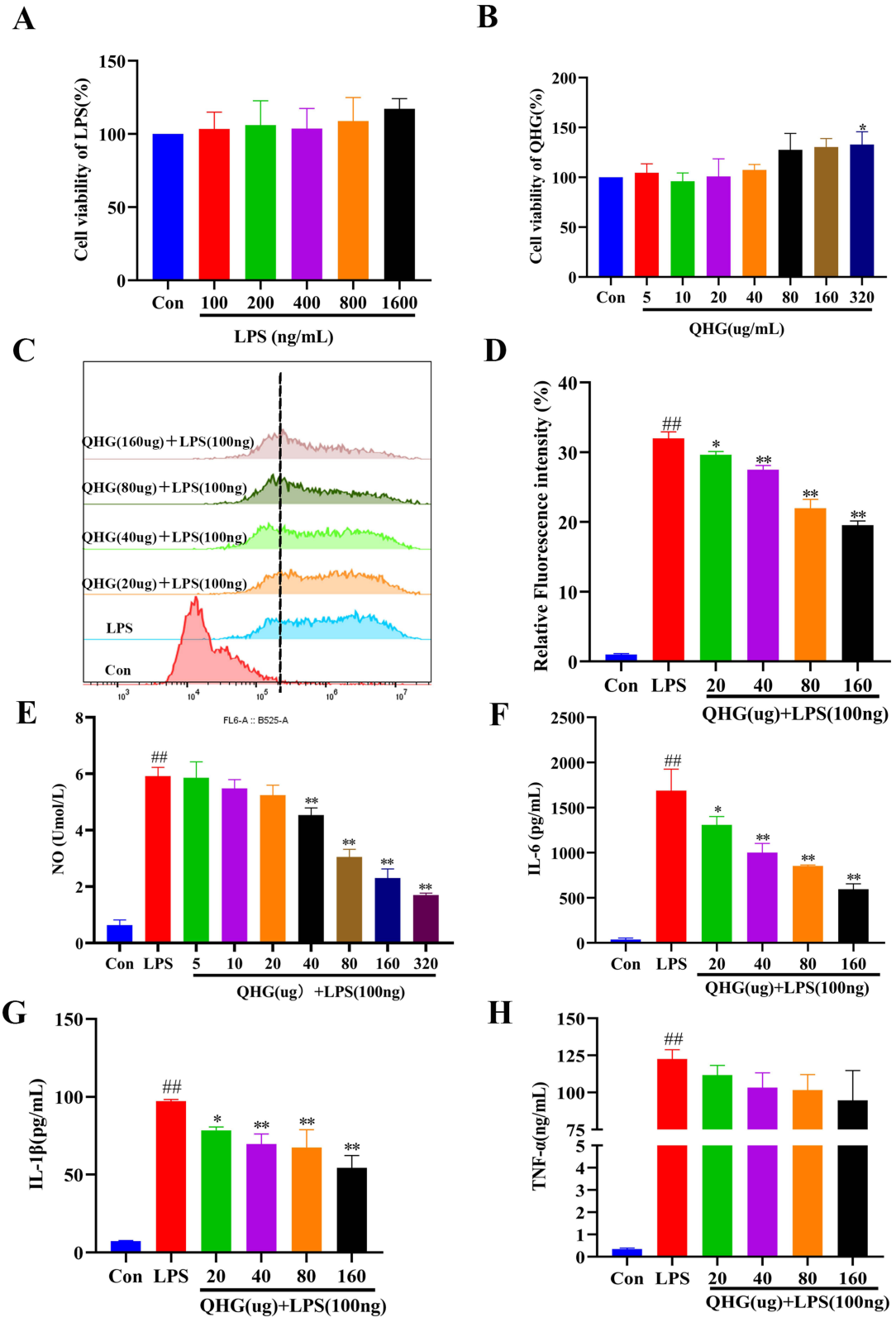

Figure 2 Effects of QHG on the secretion of NO, ROS, TNF-α, IL-6 and IL-10 in RAW264.7 cells treated with LPS. (**A**) Cell viability was determined by LPS; (**B**) Cell viability was measured by QHG; (**C** and **D**) Comparison of ROS activity in six groups; (**E**) Comparison of NO content in nine groups; (**F**) Comparison of IL-6 content in six groups; (**G**) Comparison of IL-1β content in six groups; (**H**) Comparison of TNF-α content in six groups. These data are represents as mean ± SD (n=3-4). ns $P > 0.05$. Compared with the control group *$p < 0.05$, **$p < 0.01$; compared with the LPS group $^{\#\#}p < 0.01$.

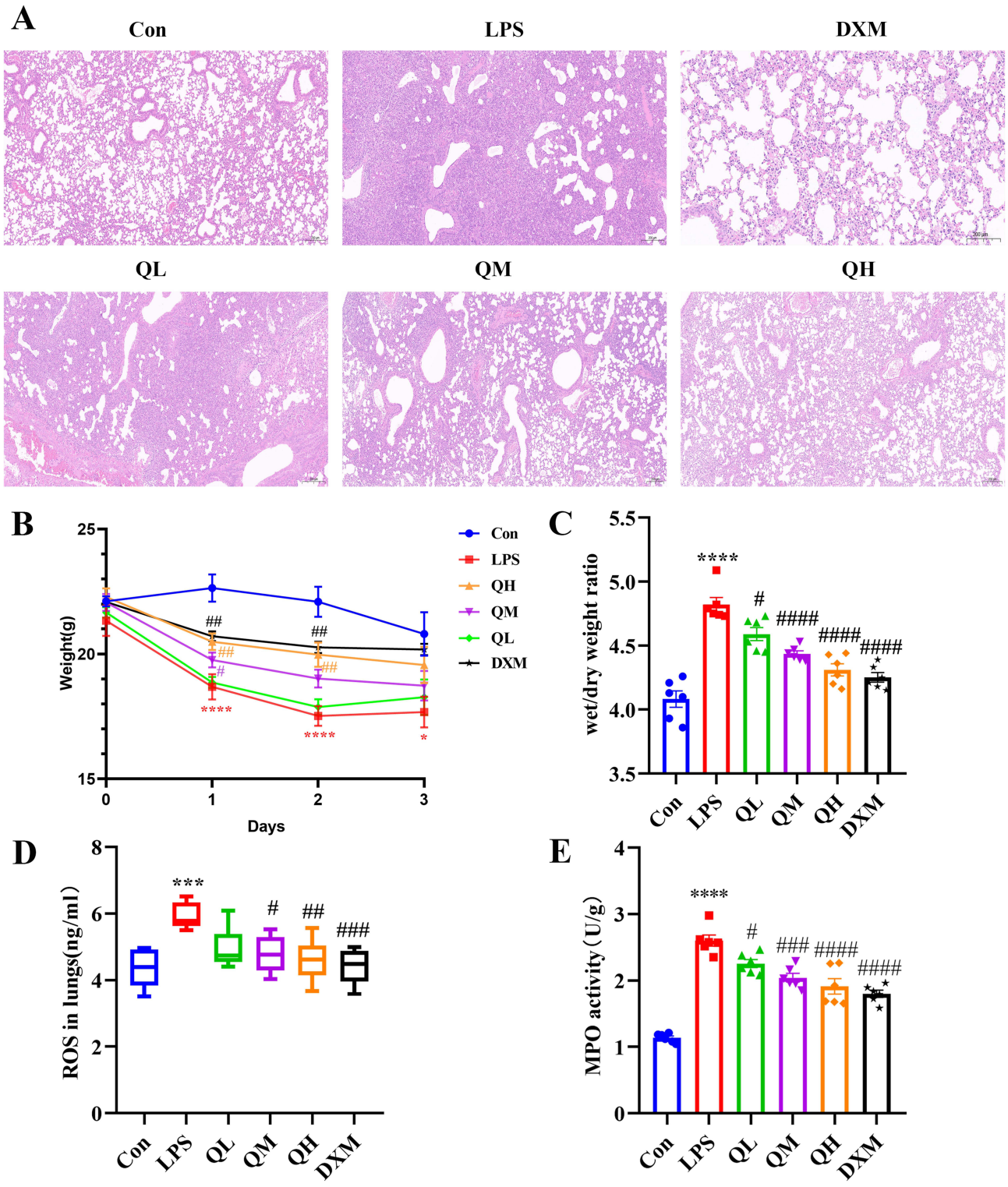

Figure 3 Protective effects of QHG on LPS-induced ALI in mice. (**A**) H&E result of lung tissue for histopathologic analysis (scale bar = 200 μm); (**B**) Body weight; (**C**) W/D ratio; (**D**) ROS viability in lung; (**E**) MPO viability in lung. These data are represents as mean ± SD (n=6). ns P > 0.05. Compared with the control group *p < 0.05, ***p < 0.001, ****p < 0.0001; compared with the LPS group $^{\#}$p < 0.05, $^{\#\#}$p < 0.01, $^{\#\#\#}$p < 0.001, $^{\#\#\#\#}$p < 0.0001.

Transcriptomics Analysis of QHG

PCA was conducted using the R software. PCA results indicated distinct separation among the control, LPS, and QH groups, revealing notable differences in gene expression in the lung tissues of ALI mice compared with controls

https://doi.org/10.2147/JIR.S523490

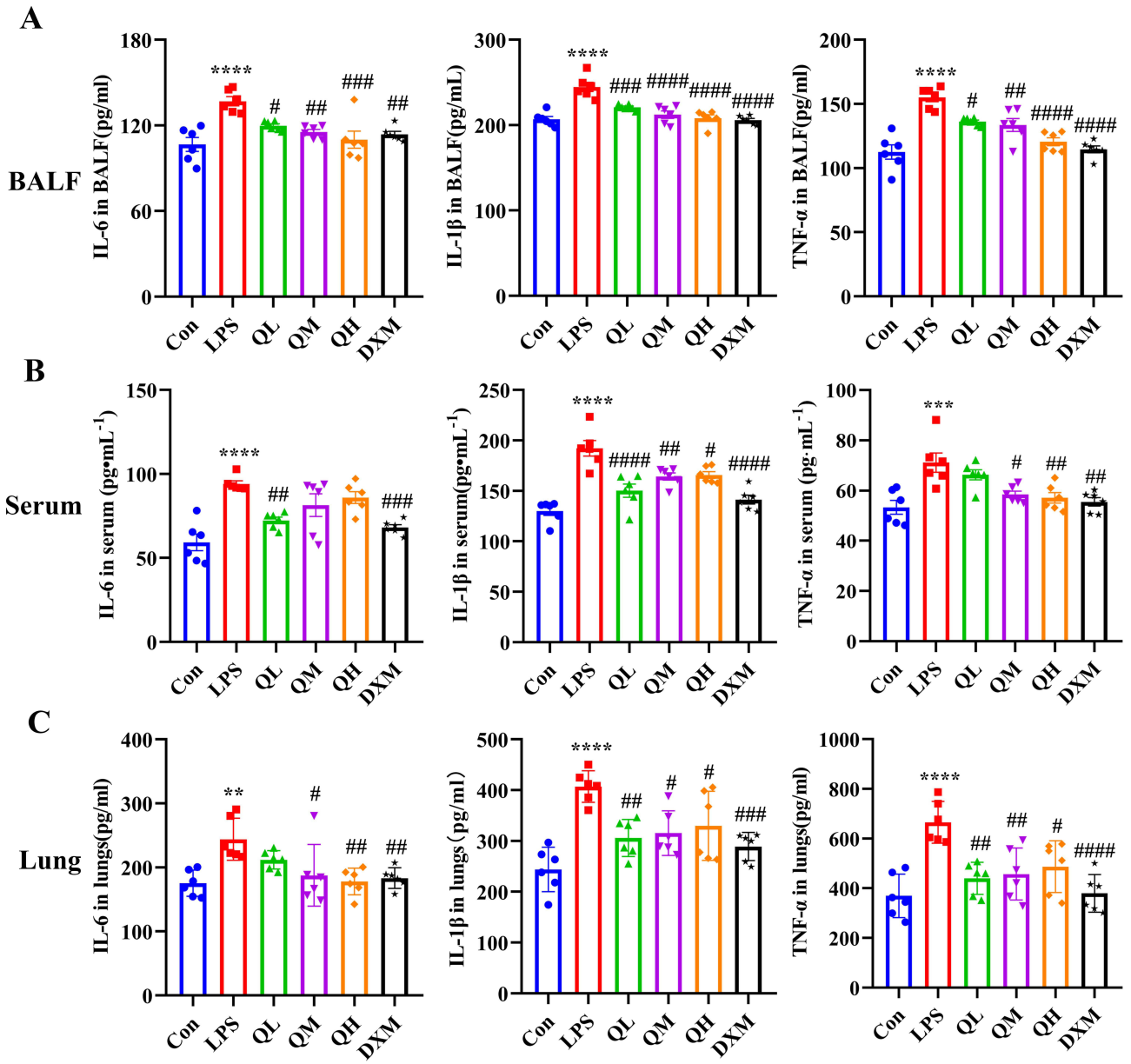

Figure 4 QHG suppressed inflammatory cytokine. (**A**–**C**) Inflammatory cytokines content in BALF, serum and lung tissues. These data are represents as mean ± SD (n=6). ns P > 0.05. Compared with the control group **p < 0.01, ***p < 0.001, ****p < 0.0001; compared with the LPS group $^{\#}$p < 0.05, $^{\#\#}$p < 0.01, $^{\#\#\#}$p < 0.001, $^{\#\#\#\#}$p < 0.0001.

(Figure 5A). A marked reversal in gene expression was observed after QH treatment. Differentially expressed genes (DEGs) were identified using DESeq2 software between two different groups with the parameter set to false discovery rate (FDR) < 0.05 and absolute fold change (FC) ≥ 2.[28] Compared to the control group, 5433 DEGs were identified in the LPS group, with 1976 upregulated and 3457 downregulated genes. QH and LPS treatment resulted in the identification of 127 DEGs, including 60 upregulated and 67 downregulated genes (Figure 5B). Further analysis included differential volcano plots based on DEG data for each control group (Figure 5C and D). To identify affected pathways, KEGG enrichment circle maps (Figure 5E and F) and bubble maps (Figure 5G and H) were generated. The purple plates, representing metabolism, showed significant increases for both LPS and QH treatments (Figure 5E and F), indicating that QH-induced changes in biological function may concentrate on metabolites in the ALI mouse model. A total of 120 KEGG pathways were enriched by QH and LPS treatments, with the top 13 most significant pathways presented as scatter plots (Figure 5H). Notably enriched pathways included the "NLR signaling pathway", "hepatitis C", "measles",

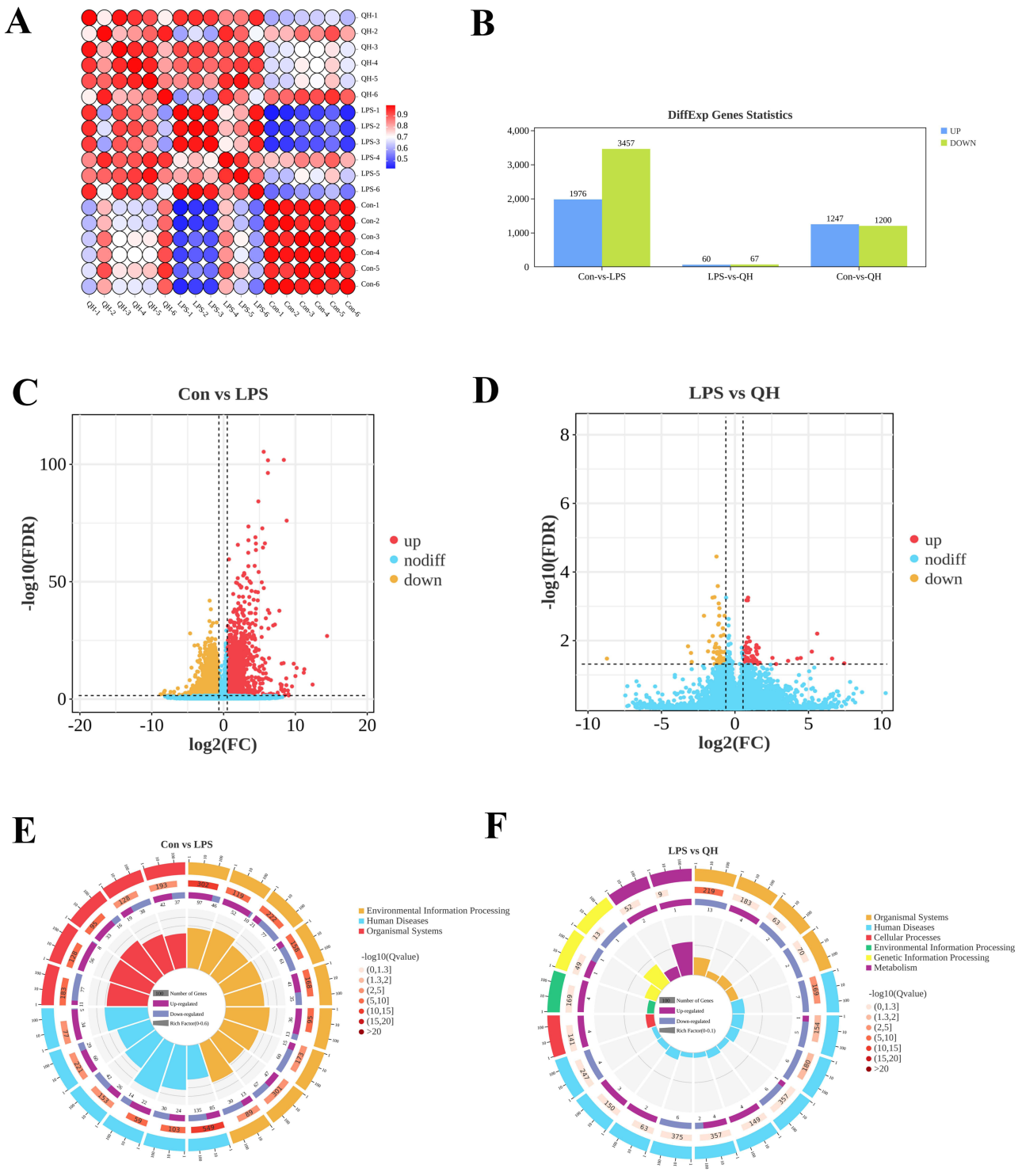

Figure 5 Continued.

https://doi.org/10.2147/JIR.S523490

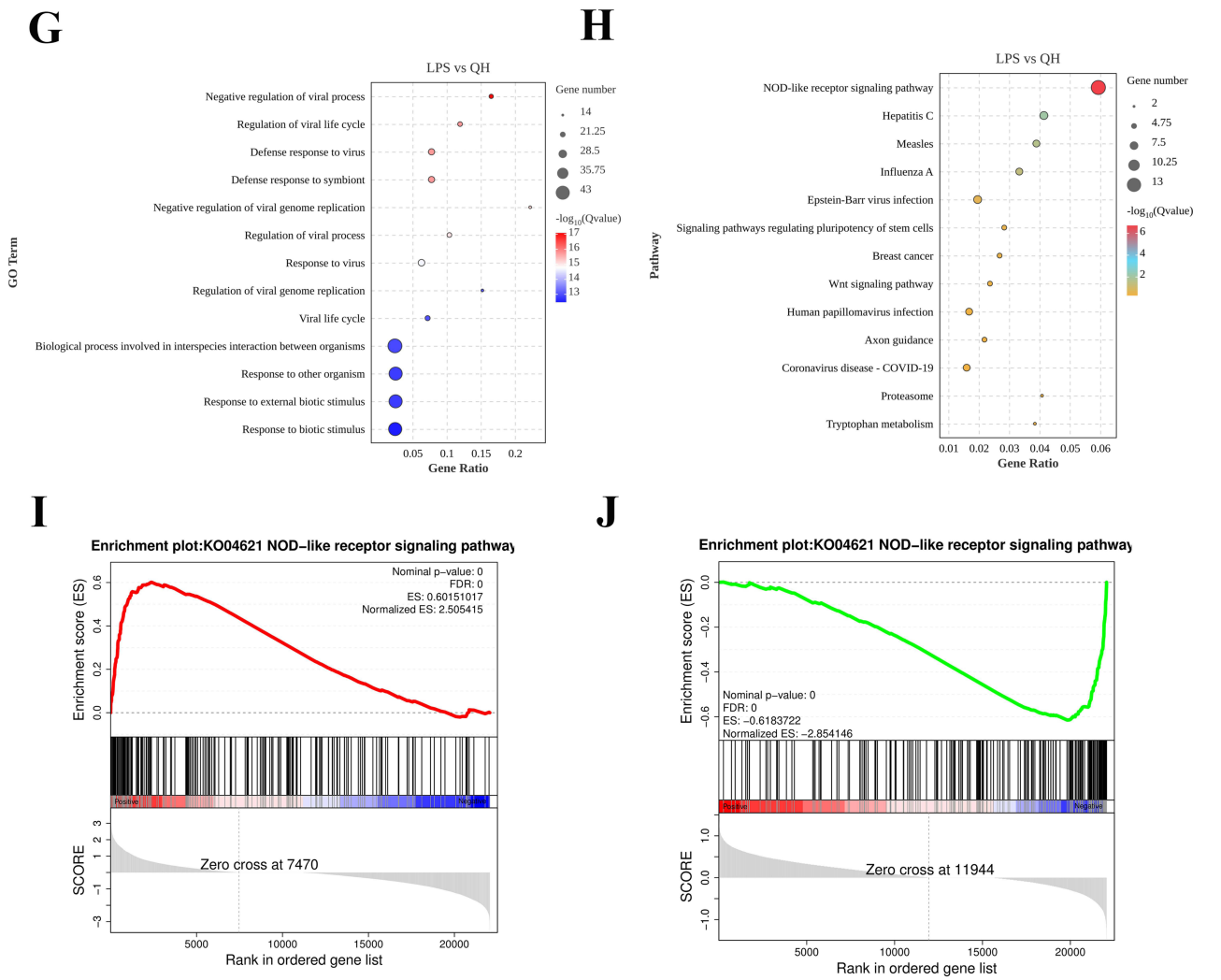

Figure 5 Transcriptomics analysis treated with QH in mice. (**A**) Show the PCA scores plots of control, LPS and QH groups; (**B**) Show the differential gene data statistical map; (**C** and **D**) Show the volcano map DEGs of control, LPS and QH groups; (**E** and **F**) Show the KEGG enrichment diagram of control, LPS and QH groups; (**G** and **H**) GO and KEGG enrichment analysis for DGEs of LPS vs QH; (**I** and **J**) GSEA enrichment analysis about the NOD-like signaling pathway, in GESA for Con vs LPS, LPS vs QH.

"influenza A", and "Epstein-Barr virus infection", all with statistical significance at $p < 0.01$. These findings suggested that QHG may affect these specific pathways, leading to reduced ALI symptoms in mice.

Gene Set Enrichment Analysis (GSEA) of the NLR signaling pathway revealed an overall upregulation trend in the LPS vs control group (Figure 5I and J). After QH treatment, a significant downregulation was observed in most of the upregulated genes. By analyzing these genes Collectively within the NLR pathway, Nampt, Casp4, Nfkbia, IL-6, Cxcl1, Cxcl2, Ikbke, Nod2, Tnfaip3, Nlrp3, Mefv, Birc3, and Gsdmd might play crucial regulatory roles in modulating this pathway. Therefore, it is reasonable to speculate that QH potentially exerts a protective effect against LPS-induced ALI in mice by stimulating the interplay between signaling pathways through its influence on relevant genes within the NLR signaling pathway. However, the precise mechanism by which QH alleviates LPS-induced ALI via the NLR signaling pathway warrants further investigation.

Effects of QHG on NLR Signaling Pathway Activation in ALI Mouse Lung Tissues

GSEA highlighted the involvement of crucial proteins in the NLR signaling pathway, such as Caspase-1, ASC, IL-1β, GSDMD, and NLRP3. Western blot analysis and qRT-PCR analysis, depicted in Figure 6, confirmed that QH significantly suppressed LPS-induced increase in Caspase-1, NLRP3, and IL-1β levels, QH can reduce the expression of IL-18 in mRNA. Protein expression was assessed in mouse lung tissue, and immunofluorescence results (Figure 7) showed a significant reduction in the expression of ASC, GSDMD, IL-1β, NLRP3, and Caspase-1 in the QH group compared to that in the LPS group. Immunohistochemical findings (Figure 8) further supported that the protein levels of ASC, GSDMD, IL-1β, NLRP3, and Caspase-1 were markedly lower in the QH group than in the LPS group, indicating the substantial inhibitory effect of QH on key proteins in the NLR signaling pathway.

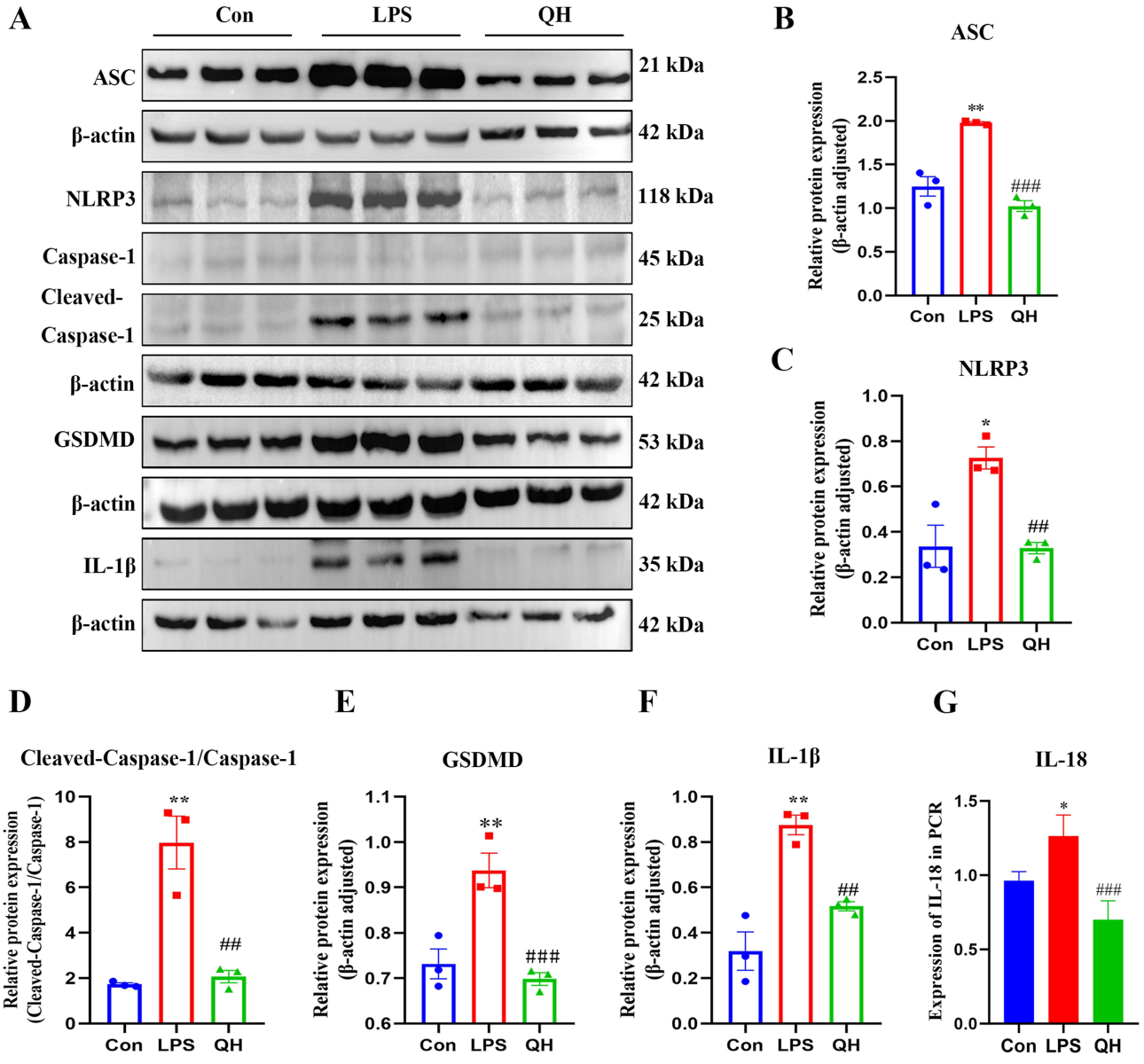

Figure 6 Western blots and quantification. (**A**) Western blots of ASC, GSDMD, IL-1β, NLRP3, Caspase-1 in each group of mice lungs. (**B–F**) The expression levels of ASC, GSDMD, IL-1β, NLRP3, Caspase-1 proteins in mice lungs. (**G**) The mRNA expression levels of IL-18 in mice lungs. These data are represents as mean ± SD (n=3). ns $P > 0.05$. Compared with the control group *$p < 0.05$, **$p < 0.01$; compared with the LPS group $^{\#\#}p < 0.01$, $^{\#\#\#}p < 0.001$.

https://doi.org/10.2147/JIR.S523490

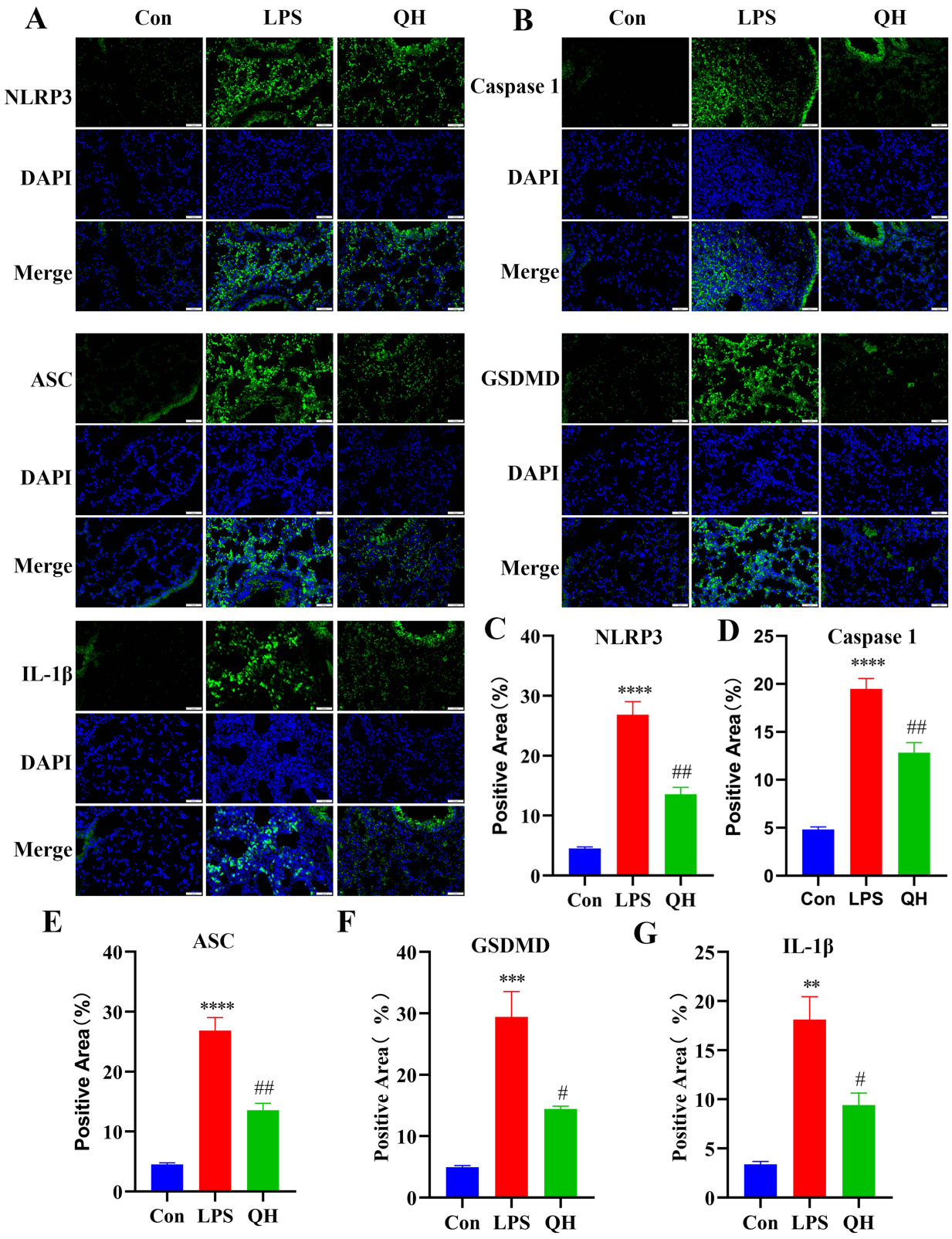

Figure 7 Immunofluorescence and quantification. (**A** and **B**) Representative immunofluorescence for ASC, GSDMD, IL-1β, NLRP3, Caspase-1 after DAPI staining in mice lungs. Scale bar: 50μm. (**C**–**G**) The quantification of positive area in mice lung. These data are represents as mean ± SD (n=3). ns $P > 0.05$. Compared with the control group $^{**}p < 0.01$, $^{***}p < 0.001$, $^{****}p < 0.0001$; compared with the LPS group $^{\#}p < 0.05$, $^{\#\#}p < 0.01$.

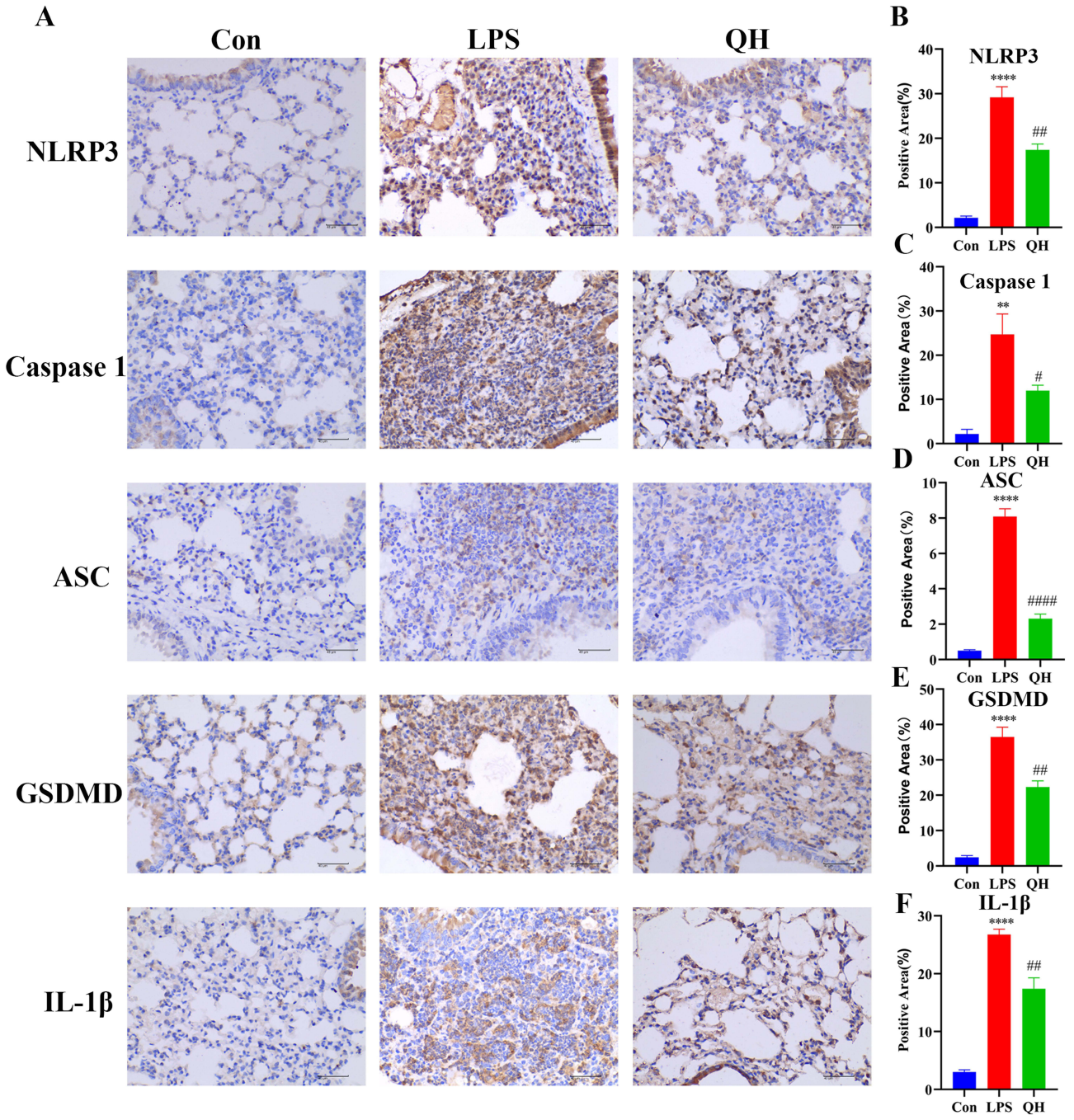

Figure 8 Immunohistochemical and quantification. (**A**) Representative immunostaining for ASC, GSDMD, IL-1β, NLRP3, Caspase-1 in mice lungs. Scale bar: 40 μm. (**B–F**) Quantification of ASC, GSDMD, IL-1β, NLRP3, Caspase-1 fluorescence intensity in six groups. These data are represents as mean ± SD (n=3). ns P > 0.05. Compared with the control group $^{**}p < 0.01$, $^{****}p < 0.0001$; compared with the LPS group $^{\#}p < 0.05$, $^{\#\#}p < 0.01$, $^{\#\#\#\#}p < 0.0001$.

Discussion

Following the onset of ALI, a rapid inflammatory response results in endothelial cell damage and epithelial barrier dysfunction, and further promotes immune cell infiltration into the lung interstitium and alveoli. Macrophages and neutrophils involved in this process produce excessive pro-inflammatory cytokines, leading to a cytokine storm. This reaction increases the permeability of pulmonary microvessels and causes pulmonary edema, resulting in severe lung injury and multiple organ dysfunction.[29–31] Recent research has demonstrated that TCM offers distinct therapeutic advantages in the treatment of ALI.[32–34] Clinically, QHG effectively treats numerous patients with upper respiratory

https://doi.org/10.2147/JIR.S523490

tract infections, particularly influenza. Therefore, it is hypothesized that QHG has potential therapeutic effects on ALI in mice, and its pharmacodynamics and mechanisms of action are currently being investigated through relevant experiments.

HPLC analysis identified seven primary chemical components of QHG. The anti-inflammatory activity of cryptochlorogenic acid may inhibit LPS-induced inflammatory responses via the Nrf2/HO-1 signaling pathway in RAW 264.7 macrophages.[35] Similarly, Forsythiin A has been reported to alleviate ALI by reducing inflammation and restoring the integrity of the lung and colon epithelial barriers via the PPAR-γ/RXR-α pathway.[36] Isochlorogenic acid A was identified, which has the ability to inhibit the Nf-κB/NLRP3 signaling pathway, thereby reducing ALI.[37] In a mouse model of LPS-induced ALI, QHG significantly reduced IL-6, IL-1β, and TNF-α levels in the serum, alveolar lavage fluid, and lung tissues, potentially mitigating of ALI-related injury.[38,39] In this context, pathological findings also demonstrated that QHG remarkably ameliorated ALI-induced pathological changes by mitigating edema and the infiltration of inflammatory cells within the lung tissue, thereby reducing hemorrhage. The rupture of inflammatory factors leads to an imbalance in the oxidative and antioxidant mechanisms of the lungs, which increases oxidative stress and induces apoptosis.[40,41] MPO and SOD levels are indicators of lung tissue inflammation.[42] In the present study, QHG significantly reduced the ROS and MPO levels in the lung tissues of mice. Thus, the improvement of QHG in LPS-induced ALI may be due to the anti-inflammatory, antioxidant, and anti-apoptotic mechanisms.

Transcriptome sequencing is a powerful tool for exploring RNA expression changes in lung tissue, uncovering disease mechanisms, identifying drug targets, comprehensively understanding abnormal gene expression during ALI, and elucidating potential molecular mechanisms of QHG in ALI treatment.[43] Transcriptome analysis in this study confirmed that the NLR signaling pathway was differentially enriched, and that the anti-ALI process of QHG involved factors such as Nampt, Casp4, IL-6, Cxcl2, Nod2, Tnfaip3, Nlrp3, and gsdmd. This may indicate that these factors are crucial for improving ALI. To confirm the results of transcriptome analysis, qRT-PCR, Western blot analysis, immunohistochemistry, and immunofluorescence assays were performed. The experiments further confirmed that the NLR signaling pathway is the key pathway for the QHG treatment of ALI, and its key targets, such as Caspase-1, ASC, IL-1β, GSDMD, and NLRP3, were significantly improved in LPS-induced lung injury caused by LPS. The inflammasome is a protein complex that includes the NLR family and is very important in innate immunity. The NLRP3 inflammasome, a complex containing an N-terminal PYD, is highly representative of this pathway because of its ability to bind ASC and pro-caspase-1, thus forming the NLRP3 inflammasome. To date, activation of the NLRP3 inflammasome has been documented to result in autocleavage of caspase-1, which further cleaves pro-IL-1β and pro-IL-18 into their mature forms, IL-1β and IL-18. Caspase-1 can also promote the cleavage of GSDMD and release the inflammatory subunit GSDMD-N, thereby inducing an inflammatory response.[44] Furthermore, activation of the NLRP3 inflammasome has been associated with the acceleration of ALI.[45] This study also showed that QHG exerts its protective role in LPS-induced ALI in mice, mainly by modulating key proteins in the NLR signaling pathway, including the inhibition of inflammasome cell pyroptosis.These results suggest that QHG could be developed into a therapeutic agent for treating ALI (Figure 9). At present, our research team has established a cell pyroptosis model suitable for studying inflammasomes. In the future, we plan to investigate the effects of silencing or overexpressing the key gene NLRP3 to observe the influence of Qingwen Hufei Granules on NLRP3 inflammatory pyroptosis. The results will be verified in NLRP3 knockout model mice based on the experimental findings.

QHG was shown to suppress LPS-induced inflammatory responses in RAW264.7, inhibit peroxide reactions, and further reduce inflammatory factor production. Macrophages serve as natural immune cells for the regulation of inflammation and tissue repair, and have drawn significant research interest. Additionally, mesenchymal stem cells (MSCs) from various tissues have been shown to aid in tissue regeneration and inflammation reduction. The primary mode of MSC involvement in tissue repair is via a paracrine mechanism, particularly via exosomes. Studies have shown that alveolar macrophages are the main cellular targets of MSC-derived exosomes in mitigating lung inflammation and injury,[3,46,47] providing new directions for future QHG research. QHG can relieve wind and heat, clear the lungs, alleviate cough, and strengthen the spleen and stomach. Herbs such as DangShen (*Codonopsis pilosula* (Franch.)Nannf.), ChaoBaizhu (*Atractylodes macrocephala* Koidz.), and FuLing (*Poria cocos* (Schw.) Wolf) help strengthen and protect the acquired roots. In the realm of TCM, recent years have seen a growing acknowledgment among experts of the theory concerning the interconnectedness of viscera, especially the concept that "the lung and large intestine are interior-

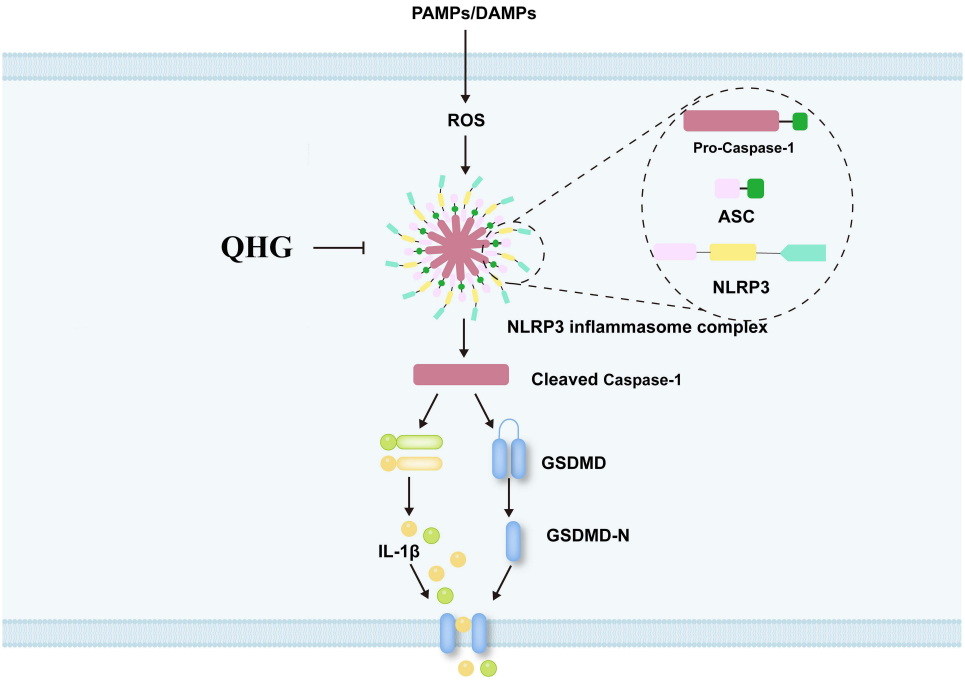

Figure 9 Mechanism of QHG in the alleviation of ALI. "⊣" means QHG can inhibit NLRP3 inflammasome-dependent pyroptosis. "→" means PAMPs/DAMPs can activate key genes on the NOD-like signaling pathway.

exteriorly related", in managing respiratory ailments. Stemming from this concept, the "lung-gut axis" theory has been proposed to further understand and treat respiratory diseases. The mechanism of action is primarily reflected in the regulation of bacterial metabolism and immune mechanisms of intestinal microorganisms.[48–50] Therefore, future research on the QHG can be based on the "lung-gut axis" theory.

Conclusion

In conclusion, our study indicated that QHG attenuates lipopolysaccharide-induced acute lung injury by suppressing NLRP3 inflammasome-dependent pyroptosis. Inhibition of the NLR signaling pathway is one of the mechanisms by which QHG affects ALI treatment.

Abbreviations

QHG, Qingwen Hufei granules; ALI, acute lung injury; TCM, traditional Chinese medicine; LPS, lipopolysaccharide; NLR, NOD-like receptor; ARDS, acute respiratory distress syndrome; GO, gene ontology; KEGG, Kyoto Encyclopedia of Genes and Genomes; HPLC, high-performance liquid chromatography; H&E, hematoxylin and eosin; BALF, bronchoalveolar lavage fluid; ROS, reactive oxygen species; DXM, dexamethasone; QL, low-QHG; QM, medium-QHG; QH, high-QHG; Myeloperoxide (MPO).

Funding

This study was supported by Shaanxi Province key research and development plan project (No. 2022ZDXM-SF-06, No. 2024SF-YBXM-489); Shaanxi Provincial Administration of Traditional Chinese Medicine COVID-19 special (No. ZYJXG-L23002); Qin Chuangyuan traditional Chinese medicine innovation research and development transformation project (No. 2022-QCYZH-006); Shaanxi Science and Technology Association youth talent lifting program project (No. 20230321); Xi'an Science and technology plan project (No. 23YXYJ0142, No. 23CXLHTJSGG0004-2023); Cao Liping national famous traditional Chinese medicine inheritance studio; Shaanxi Administration of Traditional Chinese Medicine Project (No. SZY-KJCYC-2025-ZY-006);National Administration of Traditional Chinese Medicine Project for Enhancing the Innovation Capacity of TCM (No. GHC-2024-ZFGM-396).

Disclosure

Kaihua Long and Yun Yang are co-first authors for this study. The authors declare no conflicts of interest in this work.

References

1. Long ME, Mallampalli RK, Horowitz JC. Pathogenesis of pneumonia and acute lung injury. *Clin Sci*. 2022;136(10):747–769. doi:10.1042/CS20210879
2. Mokrá D. Acute lung injury - from pathophysiology to treatment. *Physiol Res*. 2020;69(Suppl 3):S353–S366. doi:10.33549/physiolres.934602
3. Xia L, Zhang C, Lv N, et al. AdMSC-derived exosomes alleviate acute lung injury via transferring mitochondrial component to improve homeostasis of alveolar macrophages. *Theranostics*. 2022;12(6):2928–2947. doi:10.7150/thno.69533
4. Mowery NT, Terzian WTH, Nelson AC. Acute lung injury. *Curr Probl Surg*. 2020;57(5):100777. doi:10.1016/j.cpsurg.2020.100777
5. Yu WY, Gao CX, Zhang HH, Wu YG, Yu CH. Herbal active ingredients: potential for the prevention and treatment of acute lung injury. *Biomed Res Int*. 2021;2021(1):5543185. doi:10.1155/2021/5543185
6. An Y, Zhang H, Wang R, et al. Biomarkers, signaling pathways, and programmed cell death in acute lung injury and its treatment with Traditional Chinese Medicine: a narrative review. *Eur Rev Med Pharmacol Sci*. 2023;27(21):10157–10170. doi:10.26355/eurrev_202311_34292
7. Li Z, Pan H, Yang J, et al. Xuanfei Baidu formula alleviates impaired mitochondrial dynamics and activated NLRP3 inflammasome by repressing NF-κB and MAPK pathways in LPS-induced ALI and inflammation models. *Phytomedicine*. 2023;108:154545. doi:10.1016/j.phymed.2022.154545
8. He YQ, Zhou CC, Yu LY, et al. Natural product derived phytochemicals in managing acute lung injury by multiple mechanisms. *Pharmacol Res*. 2021;163:105224. doi:10.1016/j.phrs.2020.105224
9. Liu QH, Zhang K, Feng SS, et al. Rosavin alleviates LPS-induced acute lung injure by modulating the TLR-4/NF-κB/MAPK singnaling pathways. *Int J Mol Sci*. 2024;25(3):1875. doi:10.3390/ijms25031875
10. Lv H, Liu Q, Wen Z, Feng H, Deng X, Ci X. Xanthohumol ameliorates lipopolysaccharide (LPS)-induced acute lung injury via induction of AMPK/GSK3β-Nrf2 signal axis. *Redox Biol*. 2017;12:311–324. doi:10.1016/j.redox.2017.03.001
11. Salazar-Puerta AI, Rincon-Benavides MA, Cuellar-Gaviria TZ, et al. Engineered extracellular vesicles derived from dermal fibroblasts attenuate inflammation in a murine model of acute lung injury. *Adv Mater*. 2023;35(28). doi:10.1002/adma.202210579
12. Coll RC, Schroder K, Pelegrín P. NLRP3 and pyroptosis blockers for treating inflammatory diseases. *Trends Pharmacol Sci*. 2022;43(8):653–668. doi:10.1016/j.tips.2022.04.003
13. Vande Walle L, Lamkanfi M. Drugging the NLRP3 inflammasome: from signalling mechanisms to therapeutic targets. *Nat Rev Drug Discov*. 2024;23(1):43–66. doi:10.1038/s41573-023-00822-2
14. Lv J, Gao H, Ma J, et al. Dynamic atlas of immune cells reveals multiple functional features of macrophages associated with progression of pulmonary fibrosis. *Front Immunol*. 2023;14:1230266. doi:10.3389/fimmu
15. Kilkenny C, Browne W, Cuthill IC, Emerson M, Altman DG; NC3Rs Reporting Guidelines Working Group. Animal research: reporting in vivo experiments: the ARRIVE guidelines. *Br J Pharmacol*. 2010;160(7):1577–1579. doi:10.1111/j.1476-5381.2010.00872.x
16. D'Alessio FR. Mouse Models of Acute Lung Injury and ARDS. *Methods Mol Biol*. 2018;1809:341–350. doi:10.1007/978-1-4939-8570-8_22
17. Chen H, Bai C, Wang X. The value of the lipopolysaccharide-induced acute lung injury model in respiratory medicine. *Expert Rev Respir Med*. 2010;4(6):773–783. doi:10.1586/ers.10.71
18. Zhang M, Shang L, Zhou F, et al. Dachengqi decoction dispensing granule ameliorates LPS-induced acute lung injury by inhibiting PANoptosis in vivo and in vitro. *J Ethnopharmacol*. 2025;336:118699. doi:10.1016/j.jep.2024.118699
19. Yin H, Hu J, Li Y, et al. Ethyl acetate extract of *Elsholtzia bodinieri* vaniot attenuates oxidative stress in ALI mice. *J Inflamm Res*. 2025;18:7323–7336. doi:10.2147/JIR.S522638
20. Li R, Ma Y, Wu H, et al. 4-Octyl itaconate alleviates endothelial cell inflammation and barrier dysfunction in LPS-induced sepsis via modulating TLR4/MAPK/NF-κB signaling: 4-Octyl itaconate alleviates endothelial dysfunction. *Mol Med*. 2025;31(1):240. doi:10.1186/s10020-025-01160-2
21. Zhou T, Zhang Z, Zhan Y, et al. TSLP pretreatment inhibits M1 macrophage polarization and attenuates LPS-induced iNKT cell-dependent acute lung injury. *Front Immunol*. 2025;16:1583235. doi:10.3389/fimmu.2025.1583235
22. Xu T, Xu H, Zhang J, et al. Isoferulic acid mitigates acute lung injury induced by sepsis through the inhibition of JAK2. *Phytother Res*. 2025. doi:10.1002/ptr.8526
23. Cheng X, Sun Q, Zheng R, et al. Milk-derived exosomes exert anti-inflammatory activity in lipopolysaccharide-induced RAW264.7 cells by modulating the TLR4/NF-κB and PI3K/AKT signaling pathways. *Exp Ther Med*. 2025;30(2):149. doi:10.3892/etm.2025.12899
24. Jiang S, Xu X, Deng C, et al. Pleiotropic role of TLR2-mediated signaling in the protection of psoralidin against sepsis-induced acute lung injury. *Phytomedicine*. 2025:156443. doi:10.1016/j.phymed.2025.156443
25. Wang X, Zhou Z, Li D, et al. The molecular mechanisms of imatinib treatment on acute lung injury in septic mice through proteomic technology. *J Immunol Res*. 2025;2025:4526375. doi:10.1155/jimr/4526375
26. He SY, Pan CS, Yan L, et al. Qing-Fei-Pai-Du-Tang ameliorates lipopolysaccharide-induced rat acute lung injury through attenuating pulmonary microcirculatory disturbances via multi-target regulation. *Phytomedicine*. 2025;143:156839. doi:10.1016/j.phymed.2025.156839
27. Liu Y, Wang C, Hui T, et al. Cornus officinalis loganin attenuates acute lung injury in mice via regulating the PI3K/AKT/NLRP3 axis. *J Ethnopharmacol*. 2025:120104. doi:10.1016/j.jep.2025.120104
28. Gu Y, Bai J, Zhang J, et al. Transcriptomics reveals the anti-obesity mechanism of Lactobacillus plantarum fermented barley extract. *Food Res Int*. 2022;157:111285. doi:10.1016/j.foodres.2022.111285
29. Xia W, Pan Z, Zhang H, Zhou Q, Liu Y. ERRα protects against sepsis-induced acute lung injury in rats. *Mol Med*. 2023;29(1):76. doi:10.1186/s10020-023-00670-1
30. Wu D, Liao X, Gao J, Gao Y, Li Q, Gao W. Potential pharmaceuticals targeting neuroimmune interactions in treating acute lung injury. *Clin Transl Med*. 2024;14(8):e1808. doi:10.1002/ctm2.1808
31. Li X, Wei Y, Li S, et al. Zanubrutinib ameliorates lipopolysaccharide-induced acute lung injury via regulating macrophage polarization. *Int Immunopharmacol*. 2022;111:109138. doi:10.1016/j.intimp

32. Wang Y, Yuan Y, Wang W, et al. Mechanisms underlying the therapeutic effects of Qingfeiyin in treating acute lung injury based on GEO datasets, network pharmacology and molecular docking. *Comput Biol Med*. 2022;145:105454. doi:10.1016/j.compbiomed
33. Wang Y, Wang X, Li Y, et al. Xuanfei Baidu Decoction reduces acute lung injury by regulating infiltration of neutrophils and macrophages via PD-1/IL17A pathway. *Pharmacol Res*. 2022;176:106083. doi:10.1016/j.phrs
34. Li X, Li W, Zang C, et al. Hua-Shi-Bai-Du decoction inactivates NLRP3 inflammasome through inhibiting PDE4B in macrophages and ameliorates mouse acute lung injury. *Phytomedicine*. 2024;134:155985. doi:10.1016/j.phymed.2024.155985
35. Zhao XL, Yu L, Zhang SD, et al. Cryptochlorogenic acid attenuates LPS-induced inflammatory response and oxidative stress via upregulation of the Nrf2/HO-1 signaling pathway in RAW 264.7 macrophages. *Int Immunopharmacol*. 2020;83:106436. doi:10.1016/j.intimp.2020.106436
36. Wang J, Xue X, Zhao X, et al. Forsythiaside A alleviates acute lung injury by inhibiting inflammation and epithelial barrier damages in lung and colon through PPAR-γ/RXR-α complex. *J Adv Res*. 2024;60:183–200. doi:10.1016/j.jare
37. Wang Q, Xiao L. Isochlorogenic acid A attenuates acute lung injury induced by LPS via Nf-κB/NLRP3 signaling pathway. *Am J Transl Res*. 2019;11(11):7018–7026.
38. Ding Z, Zhong R, Yang Y, et al. Systems pharmacology reveals the mechanism of activity of Ge-Gen-Qin-Lian decoction against LPS-induced acute lung injury: a novel strategy for exploring active components and effective mechanism of TCM formulae. *Pharmacol Res*. 2020;156:104759. doi:10.1016/j.phrs
39. Chen Y, Peng M, Li W, et al. Inhibition of inflammasome activation via sphingolipid pathway in acute lung injury by Huanglian Jiedu decoction: an integrative pharmacology approach. *Phytomedicine*. 2022;107:154469. doi:10.1016/j.phymed
40. Yang H, Lv H, Li H, Ci X, Peng L. Oridonin protects LPS-induced acute lung injury by modulating Nrf2-mediated oxidative stress and Nrf2-independent NLRP3 and NF-κB pathways. *Cell Commun Signal*. 2019;17(1):62. doi:10.1186/s12964-019-0366-y
41. Cui YR, Qu F, Zhong WJ, et al. Beneficial effects of aloperine on inflammation and oxidative stress by suppressing necroptosis in lipopolysaccharide-induced acute lung injury mouse model. *Phytomedicine*. 2022;100:154074. doi:10.1016/j.phymed.2022.154074
42. Liu PY, Chen CY, Lin YL, et al. RNF128 regulates neutrophil infiltration and myeloperoxidase functions to prevent acute lung injury. *Cell Death Dis*. 2023;14(6):369. doi:10.1038/s41419-023-05890-1
43. Kang ZY, Huang QY, Zhen NX, et al. Heterogeneity of immune cells and their communications unveiled by transcriptome profiling in acute inflammatory lung injury. *Front Immunol*. 2024;15:1382449. doi:10.3389/fimmu.2024.1382449
44. Liang Q, Cai W, Zhao Y, et al. Lycorine ameliorates bleomycin-induced pulmonary fibrosis via inhibiting NLRP3 inflammasome activation and pyroptosis. *Pharmacol Res*. 2020;158:104884. doi:10.1016/j.phrs.2020.104884
45. Liu Y, Shang L, Zhou J, Pan G, Zhou F, Yang S. Emodin attenuates LPS-induced acute lung injury by inhibiting NLRP3 inflammasome-dependent pyroptosis signaling pathway in vitro and in vivo. *Inflammation*. 2022;45(2):753–767. doi:10.1007/s10753-021-01581-1
46. Jiao Y, Zhang T, Zhang C, et al. Exosomal miR-30d-5p of neutrophils induces M1 macrophage polarization and primes macrophage pyroptosis in sepsis-related acute lung injury. *Crit Care*. 2021;25(1):356. doi:10.1186/s13054-021-03775-3
47. Liu X, Gao C, Wang Y, Niu L, Jiang S, Pan S. BMSC-derived exosomes ameliorate LPS-induced acute lung injury by miR-384-5p-controlled alveolar macrophage autophagy. *Oxid Med Cell Longev*. 2021;2021:9973457. doi:10.1155/2021/9973457
48. Barcik W, Boutin RCT, Sokolowska M, Finlay BB. The role of lung and gut microbiota in the pathology of asthma. *Immunity*. 2020;52(2):241–255. doi:10.1016/j.immuni.2020.01.007
49. Alharris E, Mohammed A, Alghetaa H, Zhou J, Nagarkatti M, Nagarkatti P. The ability of resveratrol to attenuate ovalbumin-mediated allergic asthma is associated with changes in microbiota involving the gut-lung axis, enhanced barrier function and decreased inflammation in the lungs. *Front Immunol*. 2022;13:805770. doi:10.3389/fimmu.2022.805770
50. Saint-Criq V, Lugo-Villarino G, Thomas M. Dysbiosis, malnutrition and enhanced gut-lung axis contribute to age-related respiratory diseases. *Ageing Res Rev*. 2021;66:101235. doi:10.1016/j.arr.2020.101235